# On minimum bow force for bowed strings

Hossein Mansour[1], Jim Woodhouse*[2], and Gary P. Scavone[1]

[1]Computational Acoustic Modeling Laboratory, Schulich School of Music, McGill University, 555 Sherbrooke Street West, Montréal, Québec H3A 1E3, Canada
[2]Cambridge University Engineering Department, Trumpington Street, Cambridge CB2 1PZ, UK.

January 10, 2017

## Abstract

A famous theoretical prediction of the minimum bow force to maintain Helmholtz motion of a bowed string is re-examined to take account of effects associated with resonances of the instrument body. Starting from a more robust assumption of an ideal stick-slip velocity waveform at the bowing point rather than a perfect sawtooth-shaped excitation force at the bridge, the analysis predicts that the minimum bow force, and the force waveform exciting the instrument bridge, can depend in a complicated way on the position of the bow on the string. Also, the frequency of "maximum wolfiness" of an instrument like a cello is predicted to shift away from that of the strong body resonance causing a wolf note. Simulations are used to evaluate the new formulation. For the simple case in which the string vibrates only in a single polarisation, the results are accurately confirmed. However, simulation also reveals that string vibration in the second polarisation can change the detailed response. Further simulations are used to investigate the influence on minimum bow force of some physical details of the model, especially torsional string motion and the presence of sympathetic strings.

PACS numbers: 43.40.Cw, 43.75.De

## 1 Introduction

### 1.1 Background

When a player plucks a guitar string, almost regardless of the strength and the position of the pluck, it will lead to a "musical" guitar sound with a pitch very close to the first mode frequency of the string. By contrast, not all gestures applied to a bowed string lead to the desired "singing" sound: a bowed string is a nonlinear oscillator, capable of a richer repertoire of vibration regimes than a plucked string. This motivates the investigation of factors influencing the ease of playing, or "playability", which can be somewhat independent of questions relating directly to sound quality.

Two famous examples of playability factors are the minimum and maximum bow forces. The Helmholtz motion, the usual desired motion of a bowed string, involves a single sharp corner travelling back and forth along the string, triggering slip and stick transitions when passing underneath the bow [1]. If the player does not apply enough normal bow force, the friction may be too weak to hold the string until the corner arrives, so that an untimely slip occurs during the nominal sticking phase. This results in more than one slip per cycle and a consequent "surface" sound. On the other hand, if the bow force is too high, the bowhair's grip on the string is too strong, and the string force associated with the arrival of the Helmholtz corner may be insufficient to trigger the slip. This usually results in non-periodic motion of the string described as "raucous" or "crunchy" sound. The thresholds of bow force leading to these two types of undesirable string motion define the minimum and maximum bow force, respectively.

Early work by Raman [2], later built upon by Schelleng [3], led to simple approximate formulae for the minimum and maximum bow forces. Of these two force limits, the former makes a better candidate to account for differences between the playability of different instruments, or for the note-by-note variations on a given instrument [4]. The minimum bow force depends critically on the small but non-zero motion at the bridge of the instrument: a string that is terminated at rigid boundaries has a minimum bow force very close to zero. However, the maximum bow force is predicted to be almost independent of the properties of the body; it depends only on the properties of the string and the frictional properties of the rosin.

In the remainder of this section Schelleng's work on the minimum bow force is reviewed, together with an extension of his argument by Woodhouse [4]. In

*jw12@cam.ac.uk

the following section, the analysis is extended to a more general form involving less restrictive assumptions. The revised model predicts some significant differences of behaviour compared to the earlier work, and these predictions are verified using time-domain simulations. Finally, some particular physical details are discussed to show how they may affect the minimum bow force: torsional motion of the string, the presence of sympathetic strings, and out-of-plane vibrations of the string.

## 1.2 Schelleng's bow force limits

For an ideal Helmholtz motion, the force that the string applies to the bridge is a sawtooth waveform with the ramp slope of $T_0 v_b/\beta L$, interrupted by sudden jumps of magnitude $T_0 v_b/\beta L f_0$, where $L$ is the length of the string, $T_0$ is its static tension, $f_0$ is the stick-slip frequency of the bowed string, $v_b$ is the bow speed, and $\beta$ is the bow-bridge distance expressed as a fraction of the string length. As Schelleng argued [3], if the bridge reacts in a resistive manner with resistance $R$, its velocity would be proportional to the applied force. Integrating the sawtooth shape leads to a waveform of displacement that is parabolic within each cycle. Treating the short segment of the string between the bow and the bridge quasi-statically, such a displacement at the bridge would result in a perturbation force at the bowing point given by

$$F_{pert} = \frac{T_0^2 v_b t^2}{2R\beta^2 L^2} + K_0, \quad -\frac{1}{2f_0} < t < \frac{1}{2f_0}\,. \tag{1}$$

Time $t = 0$ is chosen to be half-way through the sticking period of the cycle. The integration constant $K_0$ can be found by enforcing the condition that the perturbation force at the bowing point is zero during the slipping phase, assuming the simple Amontons-Coulomb law of friction. The result is

$$K_0 = -\frac{v_b Z_{0T}^2}{2R\beta^2}, \tag{2}$$

where $Z_{0T} = \sqrt{T_0 m_s}$ is the characteristic impedance of the string, $m_s$ being the mass per unit length. Equation (1) then predicts a peak value of the perturbation force $-K_0$ at $t = 0$. But the perturbation force cannot exceed $F_N(\mu_s - \mu_d)$ for the Helmholtz motion to be self-consistent, where $F_N$ is the normal force of the bow on the string, and $\mu_s$ and $\mu_d$ are the static and dynamic coefficients of friction. Rearranging, the minimum bow force is thus

$$F_{min} = \frac{v_b Z_{0T}^2}{2R\beta^2(\mu_s - \mu_d)}. \tag{3}$$

Note that this criterion does not make any claims about the formation of the Helmholtz motion in the first place. In general, the formation of the Helmholtz motion is much harder than maintaining it, as is demonstrated numerically in [5].

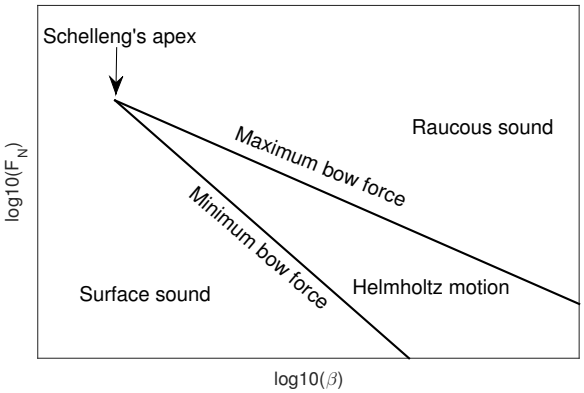


Figure 1: The "Schelleng diagram". The playable range for Helmholtz motion falls between the maximum bow force from Eq. (4) and the minimum bow force from Eq. (3).

The primary focus of this study is on the minimum bow force, but for future reference it is convenient to mention Schelleng's maximum bow force [3] as well:

$$F_{max} = \frac{2 v_b Z_{0T}}{\beta(\mu_s - \mu_d)}. \tag{4}$$

By combining Eqs. (3) and (4) Schelleng drew his now-famous diagram that shows the playable range on a log-log plot of the $F_N - \beta$ plane. A schematic of the Schelleng diagram is shown in Fig. 1: the maximum bow force line has a slope of –1, while the minimum bow force line has a slope of –2, so that the playable range becomes narrower as the bow gets closer to the bridge. The two limits will cross at some point, creating a wedge-like shape. This simple model predicts that the string will not be playable if the bow is placed closer to the bridge than the limit set by the apex of this wedge. Schelleng's diagram applies to any bowed note: there is always a minimum and a maximum bow force. For certain notes the two limits may get uncomfortably close together, in which case a player may describe the result as a "wolf note".

Schelleng himself proposed two possible enhancements of Eqs. (3) and (4). The first concerns $\mu_d$. The majority of work on the bowed string has assumed the "Stribeck" or "friction curve" model of friction, in which the friction coefficient is regarded as being a function of the instantaneous sliding speed. The maximum sliding speed in ideal Helmholtz motion is $v_b(1 - \beta)/\beta$, and if $\mu_d$ is evaluated at this velocity it becomes a function of $\beta$ and $v_b$, depending upon the shape of the particular assumed friction curve. The bow force limits then become slightly curved lines on the log-log scale [6]. Schumacher proposed a similar modification to the maximum bow force limit [7]. The correction to both minimum and maximum bow forces

tends to become less important when the player uses a larger bow speed. The friction-curve model is now known to be physically inaccurate [8, 9], so the details of this correction are subject to debate, but certainly the simple Raman-Schelleng formula requires some correction to account for the physics of friction.

The second modification that Schelleng proposed for the bow force limits is to take into account the torsional motion of the string. The friction force from the bow is applied to the surface of the string, and causes twisting of the string as well as transverse displacement. Combining the two effects, the effective characteristic impedance of the string from the bow's perspective would be $Z_{tot} = Z_{0T}Z_{0R}/(Z_{0T} + Z_{0R})$ where $Z_{0R}$ is the characteristic torsional impedance of the string. To take this effect into account in the simplest way, ignoring the dynamics of the string's torsional motion, $Z_{0T}^2$ in the numerator of the minimum bow force should be replaced with $Z_{0T}Z_{tot}$, and $Z_{0T}$ in the numerator of the maximum bow force should be replaced with $Z_{tot}$. The expected effect is a reduction in the minimum and maximum bow forces by the same factor. This issue will be investigated in some detail in Sec. 4.1.

### 1.3 Incorporating measured body behaviour

There were three restrictive assumptions involved in Schelleng's argument: (a) the excitation force at the bridge can be approximated by the sawtooth waveform resulting from a perfect Helmholtz motion; (b) the short segment of the string between the bow and the bridge can be approximated as a straight line and thus treated quasi-statically; (c) the bridge acts as a simple resistance. It can be argued that the least robust of the three is (c). To approximate the dynamics of the instrument body by a single resistance ignores the influence of the resonant modes of the body: there is no straightforward way to calculate an equivalent resistance for different instruments, or for different notes played on the same instrument.

In response to this concern, Woodhouse introduced a way to consider more realistic behaviour of the instrument body [4]. The general argument is the same as Schelleng's, except that the sawtooth excitation force is applied to the measured bridge admittance $Y(\omega)$ (the transfer function between the force and the velocity). The resulting physical velocity waveform of the bridge notch is readily calculated, based on the Fourier series decomposition of the sawtooth force waveform. The perturbation force at the bow can then be calculated by integration, again based on treating the short segment of the string quasi-statically, and finding the integration constant by imposing $F_{pert}(\pm 1/2f_0) = 0$. The minimum bow force is then found as before, by insisting that the maximum perturbation force is less than $F_N(\mu_s - \mu_d)$. It takes the form

$$F_{min} = \frac{2v_b Z_{0T}^2}{\pi^2\beta^2(\mu_s - \mu_d)} \cdot \left[ \max_t \left\{ \mathcal{R}e \sum_{n=1}^{\infty} \frac{(-1)^{n+1}}{n^2} Y(n\omega_0) e^{in\omega_0 t} \right\} + \mathcal{R}e \sum_{n=1}^{\infty} \frac{Y(n\omega_0)}{n^2} \right] \quad (5)$$

where $\omega_0 = 2\pi f_0$.

## 2 Revised minimum bow force formula

Recent simulations of bowed string motion [10] have shown that the excitation force acting on the bridge may depart significantly from the assumed perfect sawtooth waveform when the stick-slip frequency of the string falls close to a strong body resonance. This phenomenon could invalidate the first assumption made in deriving the minimum bow force relation, both by Schelleng and by Woodhouse. This may be important, because some of the most blatant playability issues arise precisely under these circumstances: playing a note close to a strong body resonance can lead to a "wolf note", especially prevalent in the cello [11, 4].

To check whether the effect seen in simulation occurs on a real instrument, the $C_2$ string of a cello with a prominent wolf note was bowed close to the frequency of the strongest body mode. The bridge force was monitored using a piezoelectric pickup system built into the top of the bridge under the string notch, similar to ones used in several previous studies [12, 13, 14]. Examples of the measured force signal are shown in Fig. 2. The hardest notes to play were found to fall in the range 171–173 Hz. The bow-bridge distance was not accurately controlled, but the bow was placed at around $\beta = 0.1$ (as can be confirmed by the spacing of the "Schelleng ripples" [15, 3] in the force signal). The upper trace in Fig. 2 shows the familiar sawtooth obtained well away from the wolf region, at a fundamental of 190.6 Hz. The middle and lower traces show the bridge forces when the fundamental falls slightly above (174.9 Hz) and slightly below (169.2 Hz) the wolf region. It can be seen clearly that the sawtooth is significantly distorted in both cases. Examining the frequency content of the bridge force (not reproduced here), the fundamental was found to be systematically weaker compared to an ideal sawtooth wave when the played note fell below the wolf region, but stronger when it fell above that range.

The effect presumably arises from interaction between the string and the body mode, and it would be useful to extend the minimum bow force calculation to capture this coupling effect. In order to stay

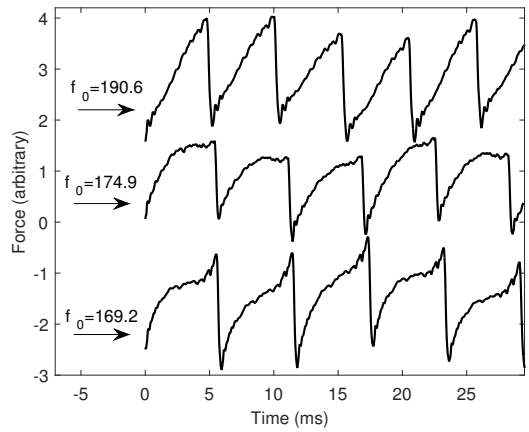


Figure 2: The bridge force measured experimentally on the $C_2$ string of a cello. The upper trace is for $f_0 = 190.6$ Hz, far away from the wolf region. The middle trace is for $f_0 = 174.9$ Hz, slightly above the wolf region, and the lower trace is for $f_0 = 169.2$ Hz slightly below the wolf region.

within the spirit of Schelleng's calculation, a different aspect of "perfect Helmholtz motion" will be assumed: in place of a perfect sawtooth bridge excitation waveform, a perfect stick-slip velocity waveform will be assumed at the bowed point. The resulting bridge force can then be calculated quite straightforwardly. Only the short length of string between bow and bridge need be included in the calculation: since the motion of the string at the bow is specified, the length of string on the finger side is effectively isolated from any influence on the bridge force (provided string rolling on the bow due to torsion is not allowed: this issue will be discussed in Sec. 4.1).

The simplest model, therefore, is to drive the body, with admittance $Y(\omega)$, through a length $\beta L$ of ideal string with properties as before. If a harmonic velocity $Ve^{i\omega t}$ is applied to the end seen from the bow, it is readily shown that the resulting force $Ge^{i\omega t}$ acting on the body is given by the transfer function

$$\frac{G}{V} = \frac{iZ_{0T}}{iZ_{0T}Y\cos k\beta L - \sin k\beta L} \tag{6}$$

where $k = \omega/c$ is the wavenumber and the wave speed $c = \sqrt{T_0/m_s}$. A more complicated version of $k$ could be used to take into account damping and bending stiffness of the string (see [16] section 4.4), but the simple version used here is in keeping with the level of approximation employed in other parts of the discussion, and by Schelleng. It is reassuring to note that this expression reverts to $1/Y$ as expected if $\beta \to 0$. If the body were to be rigid ($Y = 0$), the transfer function would become

$$\left[\frac{G}{V}\right]_{rigid} = \frac{Z_{0T}}{i\sin k\beta L} \approx \frac{Z_{0T}}{i\omega\beta L/c} = \frac{T_0}{i\omega\beta L} \tag{7}$$

where the approximate expressions apply if $\beta$ is very small. The final expression is precisely the "straight string" result used originally by Schelleng, whereby the bridge force is a scaled version of the integral of the velocity waveform. It is convenient to introduce the non-dimensional ratio of the transfer functions in Eqs. (6) and (7), which captures the correction to the bridge force arising from a non-rigid body:

$$\zeta = \frac{\sin k\beta L}{\sin k\beta L - iZ_{0T}Y\cos k\beta L}\ . \tag{8}$$

For future reference, it is useful to note the driving-point admittance at the "free" end of the string, based on the same level of approximation: this is given by

$$Y_{Tb} = -\frac{1}{Z_{0T}}\ \frac{YZ_{0T}\cos(k\beta L) + i\sin(k\beta L)}{\cos(k\beta L) + iYZ_{0T}\sin(k\beta L)}. \tag{9}$$

Including the finger side of the string, assuming an ideal string with a rigid termination, the combined driving-point admittance $Y_T(\omega)$ is then given by

$$\frac{1}{Y_T} = \frac{1}{Y_{Tb}} + iZ_{0T}\cot(k\,(1-\beta)\,L). \tag{10}$$

The rest of the argument for the minimum bow force now follows through exactly as before. A formula for the minimum bow force could be constructed directly using the Fourier series representation of the Helmholtz velocity waveform and the transfer function from Eq. (6), but it is simpler to say that the original formula Eq. (5) still applies, except that everywhere that $Y$ appears it should now be replaced by $\zeta Y$. The modified minimum bow force thus takes the form

$$F_{min} = \frac{2v_bZ_{0T}^2}{\pi^2\beta^2(\mu_s-\mu_d)}\cdot \left[\begin{array}{l} \max_t\left\{\mathcal{R}e\sum_{n=1}^{\infty}\frac{(-1)^{n+1}}{n^2}\zeta(n\omega_0)Y(n\omega_0)e^{in\omega_0 t}\right\} \\ +\mathcal{R}e\sum_{n=1}^{\infty}\frac{\zeta(n\omega_0)Y(n\omega_0)}{n^2} \end{array}\right] \tag{11}$$

Note that, similar to the bridge admittance, parameter $\zeta$ is a complex value, so the relative phase of the excitation force and the response is automatically taken into account.

To explore the consequences of this model it is useful to express the bridge admittance in terms of the body modal properties, in the standard way. Suppose the $k$th mode has frequency $\omega_k$, Q factor $Q_k$, and

mass-normalised modal amplitude at the string notch in the plane of bowing $u_k$: then

$$Y(\omega) = \sum_k \frac{i\omega u_k^2}{\omega_k^2 + i\omega\omega_k/Q_k - \omega^2}. \tag{12}$$

Equivalently, this can be expressed in terms of the effective modal mass $M_k = 1/u_k^2$. Now focus first upon the effect of a single body mode, such as is responsible for the classic cello wolf note. A single term from the summation describes this mode, and its effect can be seen in simplest form by factorising the quadratic expression in the denominator and then expanding in partial fractions:

$$\begin{aligned} &\frac{i\omega}{M_k(\omega_k^2 + i\omega\omega_k/Q_k - \omega^2)} \\ &\approx \frac{i}{2M_k}\left\{\frac{1}{\omega + \varpi_k^*} - \frac{1}{\omega - \varpi_k}\right\} \end{aligned} \tag{13}$$

where $\varpi_k \approx \omega_k(1 + i/2Q_k)$, $*$ denotes the complex conjugate and the modal damping is assumed to be small. The first partial fraction term describes a pole at negative frequency, which can be neglected in this approximation. This leaves

$$Y \approx -\frac{i}{2M_k(\omega - \varpi_k)} \tag{14}$$

so that the modified response according to the model developed above can be rearranged into the form

$$\begin{aligned} \zeta Y &\approx -\frac{i}{2M_k(\omega - \varpi_k - \frac{Z_{0T}}{2M_k}\cot k\beta L)} \\ &\approx -\frac{i}{2M_k(\omega - \varpi_k - \frac{Z_{0T}}{2M_k}\cot \pi\beta)}. \end{aligned} \tag{15}$$

The final expression applies when frequency is controlled by a player, adjusting the length of the string to give a fundamental frequency $\omega$ so that $kL = \pi$. The expression (15) describes a single pole with the same residue as in Eq. (14), but the (complex) frequency has shifted from $\varpi_k$ to $\varpi_k + \frac{Z_{0T}}{2M_k}\cot \pi\beta$. For a player searching out a wolf note, the frequency of "maximum wolfiness" is predicted to shift upwards, by an amount that increases as the bowing point moves nearer to the bridge.

These approximate results are illustrated in Fig. 3. The chosen case has the single body resonance at 172 Hz with a Q factor of 40, and in order to show the effect in a rather extreme form, a low effective mass of 120 g is assumed. Figure 3a shows the magnitude of the function $\zeta$ for a range of values of $\beta$. It is immediately clear that the model agrees with the experimental observation that the bridge force near the fundamental frequency tends to be reduced below the body resonance, and increased above it (but note that the actual switch of behaviour occurs slightly above the body resonance frequency). Figure 3b shows the corresponding plot of the modified body admittance $|\zeta Y|$ compared to its original version $|Y|$. A single peak is seen, as predicted, moving to higher frequency as $\beta$ is reduced. The height of the peak stays fixed, exactly as predicted by Eq. (15).

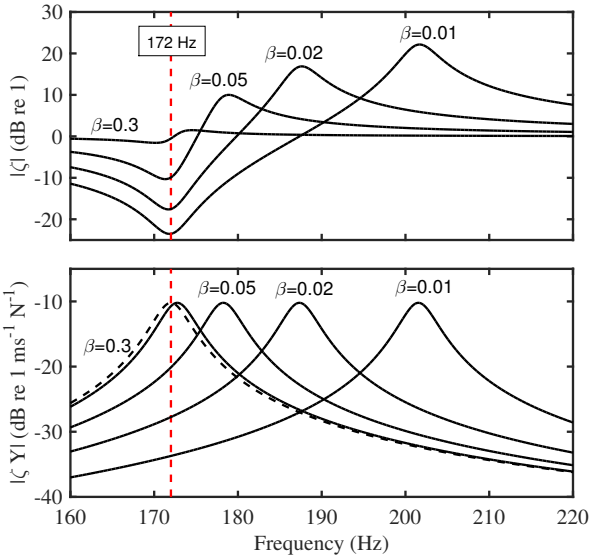


Figure 3: Effect on bridge force of a single body resonance at 172 Hz with a Q factor of 40 and effective mass of 120 g: (a) the dimensionless ratio $|\zeta(\omega)|$ defined in Eq. (15); (b) original bridge admittance $|Y(\omega)|$ (dashed line) and the modified version $|\zeta(\omega)Y(\omega)|$ for several values of $\beta$.

Figure 4 shows the simulated bridge force for the same model, in a form that is directly comparable to Fig. 2. The parameters used correspond to a bowed $C_2$ cello string [17], stopped at positions corresponding to fundamental frequencies 169.2 Hz, 174.9 Hz, and 190.6 Hz. The bow was positioned at $\beta = 1/9.21$. The general similarity between the two sets of plots is very clear.

Next, the minimum bow force as a function of the played note is calculated from Eqs. (5) and (11) and the predictions are compared against one another in Fig. 5. The same single-resonance body is assumed, and $\beta$ is fixed at 1/9.21. It can be seen that the frequency of the hardest note to play (the peak in the minimum bow force plot) is shifted upwards for the prediction made by Eq. (11). For the particular chosen value of $\beta$ this frequency is shifted from 172 Hz to 174.6 Hz. The smaller peak at around 86 Hz represents a note that has its 2nd harmonic close to the body resonance frequency.

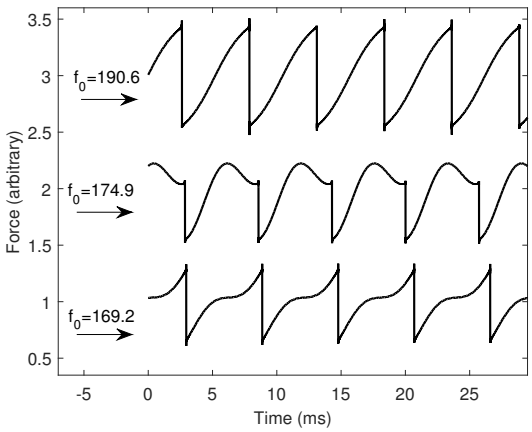


Figure 4: Simulated bridge forces for the case of a single body resonance at 172 Hz with a Q factor of 40 and effective mass of 120 g, directly comparable to ones shown in Fig. 2. The upper trace is for $f_0 = 190.6$ Hz, far away from the wolf region. The middle trace is for $f_0 = 174.9$ Hz, slightly above the wolf region, and the lower trace is for $f_0 = 169.2$ Hz slightly below the wolf region.

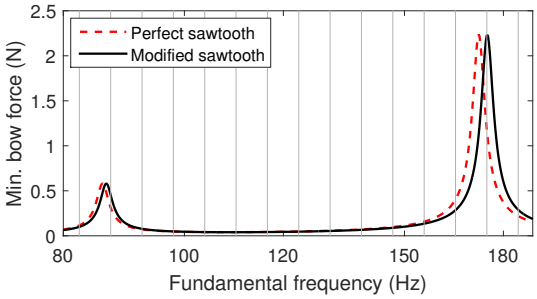


Figure 5: Calculated minimum bow force for a single-resonance body with the resonance frequency of 172 Hz. The red-dashed line shows the calculated minimum bow force predicted by Eq. (5) and the black-solid line shows the same quantity predicted by Eq. (11). The vertical lines indicate the standard frequencies of equal-tempered semitones, for reference.

# 3 Validation with time-domain simulation results

## 3.1 The perturbation force at the bow

A time-domain simulation model described in detail elsewhere [17, 18] can be used to test the modified predictions of minimum bow force. The model can include any desired combination of: the frequency-dependent damping behaviour, bending rigidity and torsional motion of the string; the coupling to body resonances and to the sympathetic strings via the bridge; both polarisations of transverse string motion; transverse and longitudinal vibrations of the bow hair ribbon, and its coupling to the bow stick. The model can also be run with different models for dynamic friction at the bow-string interface, but the simple friction-curve model is used for all simulations in this paper because the analytical results for minimum bow force assume that model.

As has been discussed in Sec. 1.2 the perturbation force at the bowing point, assuming a perfect Helmholtz motion and a resistive end support, is a parabola with its maximum value in the middle of the sticking phase. This pattern repeats every cycle, and in between each pair of parabolas is a section of slipping represented by zero perturbation force if Coulomb friction is assumed. The actual waveform of friction force, however, is much more complex. It can be influenced by the various model features listed above, and it is useful to show some examples before using simulations to address directly the question of minimum bow force: see Fig. 6.

The first notable structure in the perturbation force is the pattern of Schelleng ripples, which are a consequence of rounding of the Helmholtz corner. When the corner arrives at the bow from the finger side, it begins to interact with the bow before slipping is triggered; similarly, on the bridge side the tail of the corner continues to interact with the bow after recapture has been triggered. Those interactions occur in the sticking phase, during which the bow acts as a barrier and reflects the waves that arrive at it. That reflection requires an increase in the perturbation force at the bow, giving rise to the so-called "rabbit ears" appearing in the friction force just before and after the slipping phase [3]. These reflected waves at the bow get trapped between the bow and their corresponding termination point, and together with their counterparts from the cycles before and after, form a structure of ripples with period $\beta P$ where $P$ is the period of the full-length string [15, 3].

A consequence of the friction-curve model is that the ripples on the finger side tend to be larger than the ones on the bridge side, because they are produced by the large jump of the friction force before triggering of the slip, while the ones on the bridge side are created from the smaller jump before recapture. The effect is demonstrated in Fig. 6a, which shows the simulated friction force at the bowing point for a damped but perfectly flexible $C_2$ string terminated at rigid supports. The velocity of the string at the bowing point is also plotted, to indicate the timing of transitions between sticking and slipping. The only source of dissipation in this system is the damping of the string, which is very low; so the general trend of the friction force is flat, apart from the prominent Schelleng ripples. The arrows labelled '1' and '2' point to the "rabbit ears". $\beta$ was chosen at around 1/13, so there are 13 Schelleng ripples in each string period.

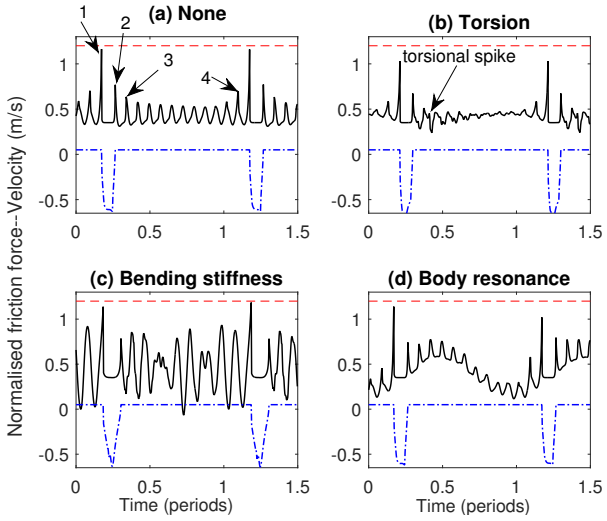


Figure 6: Samples of simulated friction force at the bowing point non-dimensionalised by the normal bow force (solid-black lines), overlaid on the synchronised string velocity at the same point (blue dashed-dotted lines). (a) is for a rigidly terminated, damped, but perfectly flexible string, and (b) to (d) are the same as (a), except in (b) the torsional motion of the string is included, in (c) the string's bending rigidity is included and in (d) the bridge is a single resonator with mode frequency of 172 Hz (the features are added individually). The simulations are made on the $C_2$ string played at 164.23 Hz with a normal bow force of 0.746 N and $\beta = 0.0764$. The red-dashed line shows the constant value of 1.2, which is the maximum value considered for the static friction coefficient.

The "rabbit ears" do not have implications for minimum bow force as they happen at the boundaries of the slipping phase. The most important ripples for triggering an early slip are probably the ones that have only been reflected once at each boundary, so that they are the least attenuated. These two ripples are shown by arrows '3' and '4' for the bridge and finger sides, respectively.

The next influence on the friction force at the bowing point is torsional motion of the string. One important effect of torsional motion is to modify the effective characteristic impedance of the string as seen by the bow. A second effect is to allow the string to roll on the bow during sticking, which allows the Schelleng ripples (or any other disturbances) arriving at the bowing point during sticking to 'leak' past the bow. This results in relatively smaller fluctuations of friction force at the bow. This effect is demonstrated in Fig. 6b, which is the same as Fig. 6a except that the torsional motion of the string has been added to the model. The ripples are much weaker, and there is also a gentle hill-like structure in the force waveform, presumably caused by the added damping of the torsional motion.

Another effect on the friction force that might conceivably be significant is the "torsional spike". The mechanism that generates "rabbit ears" also results in outgoing torsional waves. In particular, the torsional pulse initiated by the large jump in friction force at the end of sticking is sent toward the finger side. As torsional waves travel roughly five times faster than transverse waves, the pulse arrives back to the bow early in the sticking phase and causes a disturbance that could possibly trigger a slip. The spike is quite insignificant in the example waveform in Fig. 6b (marked by an arrow), but under some circumstances it can be bigger.

Bending stiffness of the string also leads to a disturbance in the friction force. It causes higher-frequency waves to travel along the string faster than low-frequency waves, so that the high-frequency content of the Helmholtz corner arrives at the bowing point before the main peak arrives, forming what can be called "precursor waves". Those precursor waves hit the bow in the nominal sticking phase, so they have to be reflected and in the process require an increased friction force at the bowing point. After a few periods, the reflected precursor waves from different cycles merge so that the individual origin of each feature cannot easily be discerned. Figure 6c shows an example: all the parameters of the model are the same as for Fig. 6a, except that the bending stiffness of the string has been added.

The final contribution to the perturbation force at the bow is the one already discussed: the motion of the bridge. Figure 6d shows an example of how a non-rigid bridge affects the friction force at the bow, all other parameters being the same as for Fig. 6a. For simplicity, a single-resonance body has been considered with a resonance frequency slightly above the played frequency of the string. The effect is a sinusoidal contribution to the friction force. For a more realistic multi-resonance case the body-induced perturbation would be a superposition of such sine waves, which is usually dominated by the strongest body resonance falling close to the string's fundamental, or one of its harmonics.

## 3.2 The playable range and sawtoothness

The results of the time-domain simulation model can now be compared with the predictions of the minimum bow force from Eq. (11), which tries to capture the effect of a non-rigid bridge. Note that among the mechanisms just illustrated, all except the trapdoor effect of the torsional waves are detrimental to the stability of the Helmholtz motion, so both original and revised predictions of minimum bow force can be expected to underestimate the minimum bow force to some extent. The predictions should give a bet-

ter match to the actual minimum bow force close to strong body resonances where the movement of the bridge is the major contributor to the perturbation force at the bow. Away from that, other effects — not accounted for in the theoretical relations — gain significance and widen the gap.

In keeping with Schelleng's original argument, for each combination of $\beta$ and $F_N$ the simulated finger-stopped $C_2$ string was initialised with Helmholtz motion and then monitored to see whether or not it could sustain that vibration regime (see [18] for details). For the purposes of this study, any motion of the string that involves only one stick and slip per string period, including "S-motion" [19], was classified as Helmholtz motion. For clarity a single body resonance was considered, using the same rather extreme case as in the results presented earlier: frequency 172 Hz, effective mass is 120 g and Q factor 40. Only a single polarisation of the string was considered. The frequency-dependent intrinsic damping of the string was based on Valette's relation [20], with parameter values taken from [17]. The stiffness of the string and its torsional motion were excluded from the model at this stage. The string was bowed with a relatively small constant bow speed of 5 cm/s.

Figure 7 shows the Schelleng diagrams calculated from the simulated data, overlaid on the theoretical maximum bow force from Eq. (4) (dashed-dotted line), minimum bow force from Eq. (5) (dashed line), and its revised version from Eq. (11) (solid line). The variation of the dynamic friction coefficient as a function of the sliding velocity has been included in the calculation of those theoretical limits. The simulations are made for 24 values of string fundamental frequency, starting from 162.35 Hz and increasing by 20-cent steps. Each subplot specifies the frequency relative to the frequency of the body mode at 172 Hz. The data points in each subplot are spaced logarithmically on the $\beta$ axis from 0.016 to 0.19 in 20 steps, and on the bow force axis from some lower limit to 11 N in 30 steps. The lower limit of bow force for each string frequency and $\beta$ value was manually adjusted, iteratively when necessary, so that it is always close but smaller than the minimum bow force at that particular combination.

The shading scheme used in Fig. 7, also calculated from the simulated data, is based on a metric to capture the extent of deviation of the calculated bridge force from being a perfect sawtooth wave. This metric (named "sawtoothness") is the relative strength of the fundamental frequency component to the second harmonic normalised by a factor 2, the value of the relative strength for a perfect sawtooth wave. Thus a perfect sawtooth has a sawtoothness of 1, while any smaller value connotes a weaker-than-expected fundamental and any larger value connotes a stronger-than-expected fundamental. Although the criterion is relatively crude, it reveals a clear and systematic pattern.

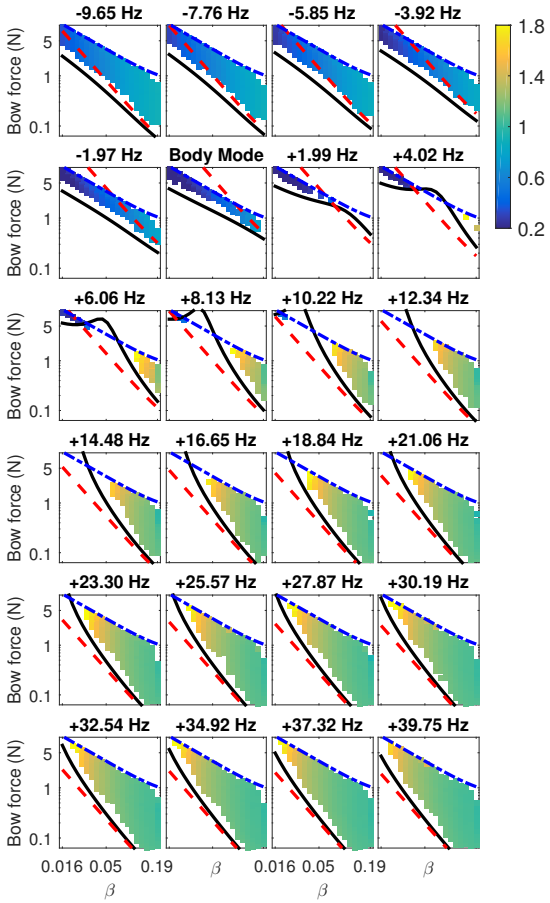


Figure 7: The Schelleng map of the playable range for a simulated damped but perfectly flexible $C_2$ cello string terminated at a single-resonance body at 172 Hz and with an effective mass of 120 g. The torsional vibrations of the string were excluded from the simulations. The number on top of each subplot shows the relative frequency of the played note with respect to the body resonance. The color of the simulated sample points represents their sawtoothness, defined in the text and according to the scale shown on the color bar. The overlaid blue dashed-dotted line shows the maximum bow force limit calculated from Eq. (4), the red-dashed line shows the minimum bow force calculated from Eq. (5), and the black-solid line is the same quantity calculated from Eq. (11).

It is immediately striking how well the revised version of the minimum bow force relation fits the lower boundary of Helmholtz motion. Both theoretical estimates slightly underestimate the minimum bow force, as anticipated, but the revised equation makes a much better prediction of the trend. Of particular interest are the range of relative frequencies -9.65 Hz to +4.02 Hz in Fig. 7 where there are many occurrences of Helmholtz motion below the level set by Eq. (5). The revised minimum bow force limit is curved in

a manner that generally avoids this situation, missing only 4 instances of Helmholtz occurrences across all simulated cases. For relative frequencies +1.99 to +8.13 Hz a local maximum occurs in the minimum bow force curve. It is encouraging to see that the $\beta$-value of this maximum depends on the fundamental frequency of the simulated string as predicted by Eq. (11), with its physical origin described by Eq. (15).

In extreme cases this local maximum crosses the maximum bow force line, with the striking consequence of splitting the playable range. These splits are plainly visible in the simulated data, following the predicted pattern in all cases (see the results for relative frequency +6.06 Hz, for instance). This phenomenon is entirely absent from Eq. (5), a difference which may well prove to be significant to a player. The maximum bow force limit set by Eq. (4) makes a very good prediction of the upper boundary of Helmholtz motion, lending credence to Schelleng's original argument. The few exceptions for which "Helmholtz motion" was achieved above that boundary were checked manually, and were confirmed to correspond to S-motion [19]. S-motion is expected to occur for $\beta$ values near, but not equal to, simple integer fractions, and it is predicted by Schelleng's argument to have a higher maximum bow force than Helmholtz motion so that it can appear in otherwise raucous territory.

The behaviour of the sawtoothness metric follows the pattern described earlier: the general rule is that at frequencies lower than the body resonance the share of the fundamental is weaker than expected, while it becomes stronger than expected at frequencies above the body resonance. There is some $\beta$-dependency as well, as is clear from the plots: the sawtoothness metric is systematically lower for small $\beta$ values, and higher for larger values. There seems to be no particular bow force dependency: the equi-sawtoothness lines are approximately vertical in each subplot. A quantitative comparison of these simulated sawtoothness results with theoretical predictions of Eq. (8) also revealed a very close agreement between the two; those results are not reproduced here.

Note that the simulations for Fig. 7 were performed for the heaviest string of the cello and with a smaller-than-normal effective body mass to show the trends in extreme form. A wide range of similar simulations have been performed with more realistic parameter values [16], not reproduced here, and in all cases the prediction of the minimum bow force from Eq. (5) was found to pass above some Helmholtz samples while the revised prediction curves correctly mirrored the simulated behaviour. There is always a tendency for the Helmholtz region to extend toward lower $\beta$ values for frequencies below the wolf region, while the Helmholtz region is reduced in the small-$\beta$ range for frequencies above the wolf region.

With a multi-resonance body, the pattern is more complicated and occurs over a wider range of frequencies as there is more than one mode contributing to the response of the body in the frequency range of interest. The playable range is not usually split into two parts for any simulated note when a more realistic model of the body is considered. All the effects become weaker, as expected, when a lighter $D_3$ string is simulated in place of a $C_2$ string.

# 4 Influences on minimum bow force

## 4.1 Torsional string motion

The simulation model can now be used to explore the effect on minimum bow force of the various additional physical effects listed earlier. As a first step, the simulations of Fig. 7 were repeated with torsional motion of the string included in the model. Figure 8 shows a comparison between the simulated data and the analytical predictions of the maximum and minimum bow forces calculated from Eqs. (4) and (11). The dashed line shows the analytical prediction of the minimum bow force when $Z_{0T}^2$ in Eq. (11) is replaced by $Z_{0T}Z_{tot}$, and the dotted line is the prediction of the maximum bow force when $Z_{0T}$ in the numerator of Eq. (4) is replaced with $Z_{tot}$, as suggested by earlier researchers [6, 7]. Interestingly, the predictions made without consideration of the torsional motion give significantly closer matches to the simulated data than the ones with such consideration. This conclusion is consistent with recent experimental findings by Mores [21] about the maximum bow force.

To understand this somewhat surprising observation, it can be argued that the influence of torsional motion on playability should manifest itself through the admittance at the bowing point as felt by the bow. In the spirit of the earlier calculations in this paper, it is easy to write down a first approximation to the combined admittance including the effect of torsional vibration. The admittance at the bowing point associated with torsional motion alone is given by

$$Y_R = \frac{1}{iZ_{0R}\left(\cot(k_R\beta L) + \cot(k_R\left(1-\beta\right)L)\right)}, \quad (16)$$

where $k_R$ is the wavenumber of torsional waves. The corresponding admittance for transverse motion alone was given in Eq. (10), and the combined admittance is simply the sum of these two. The magnitudes of the bowing-point admittances with and without allowing for torsional motion are compared in Fig. 9, and it can be seen that they are indeed very close in the lower frequency range.

The key to this observation is that the first torsional mode of the string occurs at almost five times the

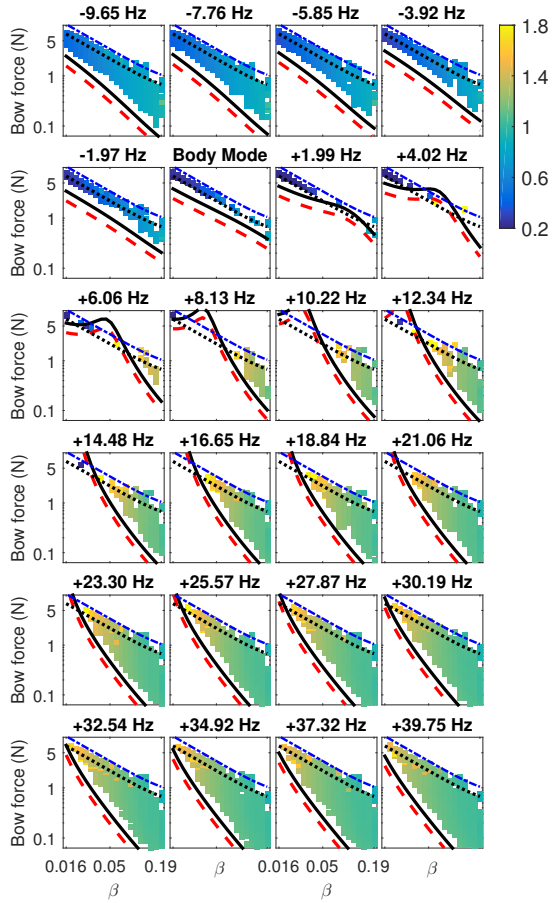


Figure 8: Same as Fig. 7 except the torsional motion of the string is included in the simulations. The blue dashed-dotted line shows the maximum bow force limit calculated from Eq. (4), the black-solid line shows the minimum bow force calculated from Eq. (11). The red-dashed line and the black-dotted lines are the minimum and maximum bow forces predictions which also take into account the torsional motion of the string as explained in the text.

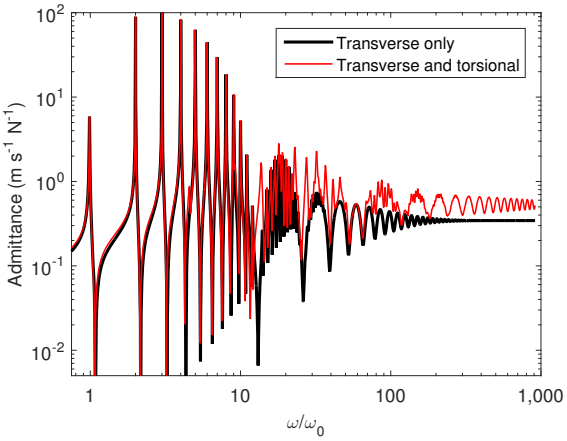


Figure 9: The magnitude of the bowing point admittance plotted against the normalised frequency. The results excluding torsional motion, from Eq. (10), are shown by the thick black line and the results including torsion as described in the text are shown by the thin red line.

stick-slip frequency of the string when it is bowed. As a result, for frequencies below the 5th harmonic of the bowed string the numerical value of $Y_R$ remains very small, so the bowing-point admittance is little affected by it. To his credit, Schumacher left the door open to this possibility noting that replacing $Z_{0T}$ by $Z_{tot}$ ignores "*the normal-modes structure of the rotational modes, thus in effect treating the string as if it were unbounded for rotational waves.*"[7].

## 4.2 Sympathetic strings

A violin or cello has four strings, of which only one is usually bowed at a given time. The other three non-played, but freely-vibrating, strings are coupled to the bowed string as well as to other freely-vibrating strings through the common bridge that supports them. For brevity these three strings can be called "sympathetic strings", although they may or may not be tuned sympathetically to the bowed string. As far as the bowed string is concerned, any effect from the sympathetic strings should come into play by modifying the bridge admittance as felt by the bowed string. The effective bridge impedance, $Z_{eff}$, is simply the sum of the bridge impedance in the absence of the sympathetic strings, plus the impedance of the sympathetic strings at the bridge:

$$Z_{eff} = \frac{1}{Y} + i \sum_{strings} Z_{0sym} \cot(k_{sym} L_{sym}), \qquad (17)$$

where the subscript "*sym*" represents the corresponding parameter for each sympathetic string. Replacing $Y$ by $1/Z_{eff}$ in all earlier equations concerning the minimum bow force gives the equivalent results with sympathetic strings taken into account.

Figure 10a shows the real part of the effective bridge admittance when a single $G_2$ sympathetic string is included. The effect in the plotted range is to add two sharp local resonance structures at around 98 Hz and 196 Hz. The admittances with and without the sympathetic string look very similar away from those frequencies. There can be some interaction between the sympathetic strings and the body resonance if they fall very close in frequency: that interaction usually results in some repulsion of the two peaks. Figure 10b shows the minimum bow force plot, equivalent to Fig. 5a but calculated using the modified admittance. Not surprisingly, the minimum bow force is most affected around 98 Hz, its almost-integer multiples, and the subharmonics of all of those multiples.

Two examples of those subharmonics visible in the range plotted here are a 65.4 Hz peak that has its 3rd harmonic coincident with the 2nd mode of the sympathetic string, and a small spike at 146.83 Hz, which is half the 3rd mode frequency of the sympathetic string.

The modified admittance always shows a dip at the exact frequency of the sympathetic string modes, accompanied by a closely spaced peak. This is familiar behaviour for any structure fitted with what is variously called a "tuned mass damper" or "tuned dynamic absorber" (see for example [22]): a very similar effect occurs when a wolf suppressor is installed on a string's after-length, tuning its frequency to match the wolf note. For the particular case of a single-resonance body, the peak always happens before the dip at frequencies below the body resonance, and after the dip at frequencies above the body resonance. This trend is necessary so that the combined set of resonances, including the sympathetic strings, obey Foster's theorem: in a driving-point response, resonances and anti-resonances always alternate [23]. Translating this into the minimum bow force plot creates an interesting shape at 98 Hz. There is a dip exactly at 98 Hz which has a peak below, reflecting what happens in the admittance at around 98 Hz; as well as another small peak slightly above 98 Hz that is the consequence of the peak at slightly above 196 Hz in the admittance curve (look at the magnified box in Fig. 10b). Care should be taken not to misattribute this double peak structure to the coupling of the bowed and the sympathetic strings, and the consequent peak splitting [24, 25]. Evidently, this double peak situation does not apply to the minimum bow force plot at around 196 Hz as the peak frequencies of the fundamental and all of its harmonics are slightly above the pure multiples of 196 Hz in the admittance.

Leaving aside those details, Fig. 10 suggests that sympathetic strings can have a significant effect on the playability of the notes that are harmonically related to them, so that it may be worth including their effect in the prediction of the minimum bow force. The qualitative effect of each sympathetic string and the magnitude of the effect depends on the properties of the bridge admittance in that frequency range, and may vary from one instrument to another. As an example, an accurate relation for the minimum bow force should make a distinction between a cello that has its body resonance near $G_3$ and one that has it near $F_3{}^{\#}$. Even if those modes were equally strong, the mode near $G_3$ is more likely to be suppressed by the presence of harmonically-related open strings.

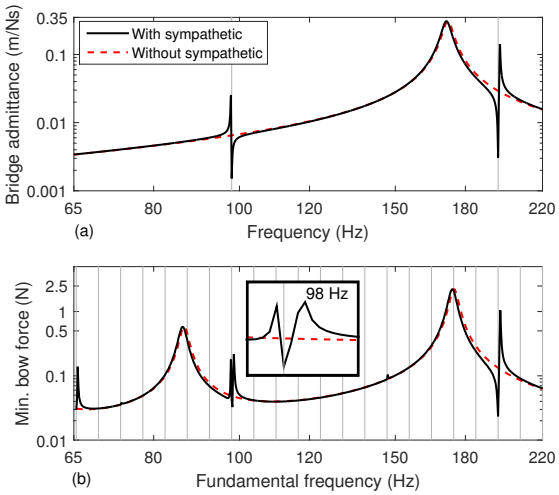


Figure 10: The bridge admittance (a) and the minimum bow force calculated from it (b) for a single-resonance body mode located at 172 Hz. The calculation of the minimum bow force is made from Eq. (11). The black-solid curve is for the case where an open $G_2$ string tuned at 98 Hz is supported on the same bridge, and the red-dashed line shows the case without the sympathetic string. The grey vertical lines in the top plot show the frequency of the sympathetic string and its 2nd harmonic, and in the bottom plot they show the musical scale spaced by a semitone. The box in the bottom plot is a zoomed version around 98 Hz. The same line types apply to both plots.

## 4.3 Out-of-plane string vibration

A string can vibrate transversely in two perpendicular polarisations. Adding a body mode with the same frequency as an unperturbed pair of string modes, the string polarisation aligned with the body mode will be effectively coupled, while the other string polarisation will be unchanged. If the unperturbed frequencies of the string and body do not exactly coincide, the coupled modes will tend to retain string-like and body-like properties, but some interaction still occurs. The degeneracy of the string modes will be broken, and each mode will have a particular polarisation direction. If the excitation from bowing is not perfectly aligned with one of these special polarisations, some vibration of the string will be induced in the plane perpendicular to the bow.

Such out-of-plane string vibration might influence minimum bow force through two quite different mechanisms. On the one hand, it will change the bowing-point admittance, and it has already been argued that this is a route for influence. On the other hand, the perpendicular string vibration will induce fluctuations in the normal force between bow and string. This will influence the friction force via Coulomb's law, or whatever other friction model that is relevant. The conditions leading to an additional slip will change, and hence the minimum bow force will change. Both effects will be briefly explored.

Looking first at the admittance at the bowing point, the presence of the two coupled string-body modes in

addition to an uncoupled string mode will result in three peaks where before there were only two. The peak that corresponds to the uncoupled vibration of the string will be rather sharp and occur at the unperturbed string frequency, while the two others will be perturbed in frequency and more heavily damped. Gough [26] has argued that the existence of the uncoupled string mode might aid the formation and stability of the Helmholtz motion as it is harmonically related to other string modes.

Consider first the single-polarisation vibration of a finger-stopped $C_2$ string with a constant Q factor of 500, and an unperturbed first mode frequency of 172 Hz, coupled to a body mode with the same unperturbed frequency, a modal mass of 120 g, a Q factor of 40, and perfectly aligned with the bowing (i.e. admittance evaluation) direction. The red-dashed line in Fig. 11a shows the admittance evaluated at $\beta = 1/13.3$ according to Eq. (10). As expected, there are two split and heavily-damped coupled modes, representing the in-phase and out-of-phase motions of the string and the bridge.

Now consider the dual-polarisation case: to give a "worst case", suppose the body mode is inclined by $\theta_M = 45°$ with respect to the admittance evaluation direction. To make the two cases compatible the mass of the body mode is reduced to $M = 120\ \cos^2\theta_M = 60$ g, so that the bridge admittance in the bowing direction would remain the same in the absence of string coupling. To find the coupled admittance, the applied force must be resolved into the coupled and uncoupled polarisation directions of the string, and the resulting velocities projected back into the evaluation direction. The admittance calculated in this way is shown by the black-solid line in Fig. 11a. Exactly as argued by Gough [26], a sharp third peak appears at the unperturbed frequency of the string. Furthermore, the coupled modes are repelled more widely than before because the effective body mass is smaller, resulting in a stronger coupling of the string and the body mode.

A point that was neglected in Gough's argument is that in order for such a sharp peak to appear in the admittance, the string needs to be free to vibrate in the out-of-plane direction, as was the case in Gough's experiments performed using electromagnetic excitation of the string in the bowing direction. However, this is not the case when a bow is in contact with the string: bow-hair coupling will significantly limit motion in the perpendicular-to-bow direction, and add damping. A more relevant bowing-direction admittance would take into account a frictionless bow remaining in contact with the string at the bowing point. This is not, of course, a practical thing to measure, but it can be calculated quite readily (see [16] for the derivation).

The blue dash-dotted line in Fig. 11a shows the result. The parameters used for the transverse vibrations of the bow-hair are extracted from [18]: a characteristic impedance of 0.79 kg/s and first mode frequency of 75 Hz for the 0.59 m full length of the bow. The Q factor is estimated at 20 for all bow-hair modes. The distance between the contact point and the frog normalised by the full length of the bow hair ribbon is chosen to be 0.31. It can be seen that the sharp uncoupled resonance has been moderately affected by the coupling to the bow-hair: its normalised frequency has been reduced from 1 to around 0.99, probably due to the added mass from the bow-hair, and it is more heavily damped as well. To put this extreme case in perspective a comparable plot is shown in Fig. 11b in which a finger-stopped $D_3$ string with an unperturbed first mode frequency of 172 Hz is coupled to a body mode with the same unperturbed frequency, but this time with a modal mass of 300 g: a more realistic value than the earlier case with mass 120 g. The body mode is inclined by $\theta_M = 20°$ and the total mass is reduced to $M = 300\ \cos^2\theta_M = 264.9$ g when both polarisations are considered. It can be seen that the unperturbed string resonance visible in the black solid line is heavily suppressed by the coupling to the bow-hair ribbon (see the blue dashed-dotted line) and is merged with the in-phase split mode near normalised frequency 0.98.

The detailed shape of the coupled admittance at the bowing point depends on many parameters, such as the mode frequencies of the bow hair, the distance of the contact point from the frog, and the static alteration of the bow-hair tension. Therefore, the particular set of parameters chosen here is not claimed to represent the exact effect that the coupling to the bow hair has on the admittance of the string. However, examination of many similar computed cases suggests that the coupled response generally remains more similar to the single-polarisation case than to the dual-polarisation case when typical body properties are considered. Any large deviation of the coupled case from the single-polarisation case would require a significant out-of-plane motion of the string, resulting in energy loss into the heavily damped ribbon of bow-hair.

Under extreme circumstances, like those shown in Fig. 11a, the effect discussed here *can* have a significant influence on the behaviour of a bowed string. Figure 12 investigates the influence of such changes in input admittance on the playable range in the Schelleng diagram, as predicted by time-domain simulations. The plot is directly comparable to Fig. 7 except that the single body mode has again been rotated to a spatial angle $\theta_M = 45°$ with respect to the bowing direction, and the already very low modal mass of 120 g has been reduced to 60 g as before, in order to preserve the effective mass in the bowing direction. The fluctuations of the bow force are not considered in the calculation of friction. The simulated results are very significantly changed as a result of including the second polarisation, and the pattern no longer matches

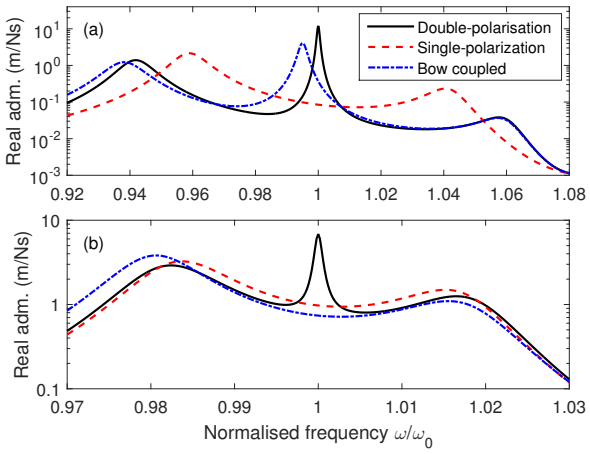


Figure 11: The real part of the input admittance at the bowing point, evaluated at $1/13.3^{th}$ of the string length away from the bridge. Red-dashed line shows the case for the single-polarisation vibration of the string, black-solid line shows the case for dual-polarisation, and the blue dashed-dotted line is the same as the dual-polarisation case except that a frictionless bow is kept in contact with the string. Both unperturbed string and body resonances are located at the normalised frequency of 1. (a) is for a $C_2$ cello string coupled to a body mode with an effective mass of 60 g and a spatial angle of $\theta_M = 45°$, and (b) is for a $D_3$ cello string coupled to a body mode with an effective mass of 264.9 g and a spatial angle of $\theta_M = 20°$. Note the different scaling of the two plots. The same line types apply to both plots.

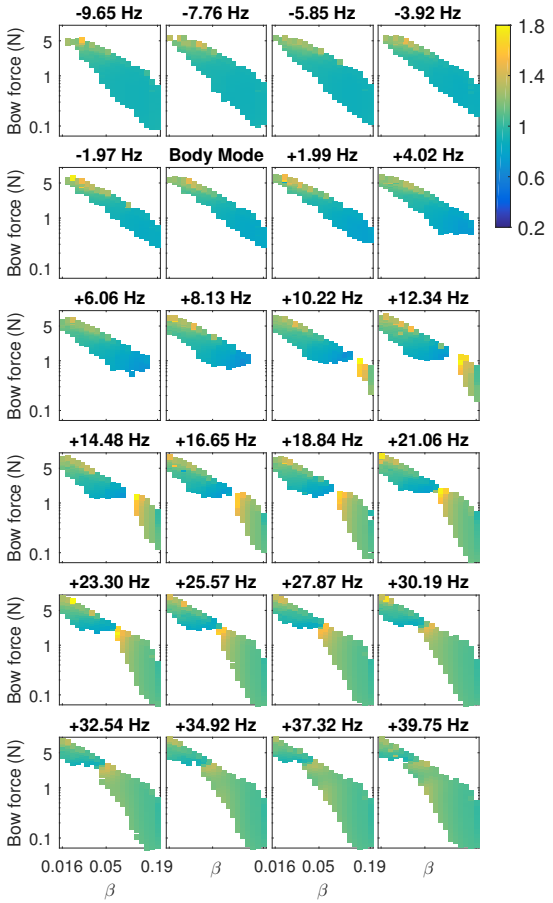


Figure 12: Same as Fig. 7 except the body mode has a spatial angle of $\theta_M = 45°$ with respect to the bowing direction. The effective body mass is reduced from 120 g to 60 g so that the effective mass in the bowing direction remains the same. The second polarisation of the string is coupled to the bow hair ribbon in its transverse direction, but the fluctuations of the bow force are not considered in the calculation of friction.

the prediction from the earlier analysis. The playable range still shows significant variation with $\beta$, but the details have been changed by the altered string-body coupling, associated with the reduced effective modal mass. There does not seem to be any simple way to derive a prediction for the minimum bow force in the dual-polarisation case, in the spirit of Schelleng's formula and the earlier analysis, so for the moment at least, simulation is the only way to get information about this effect.

As noted earlier, under more typical circumstances the second polarisation of the string appears to have only a small effect on the admittance at the bowing point via the mechanism discussed above. There is, however, a second mechanism for influence via fluctuations in the bow force. It was shown in an earlier paper [18] that adding the second polarisation resulted in fluctuations of bow force up to 10% of the nominal value, which in turn led to a significantly lower minimum bow force for the particular case studied. Qualitatively, the effect of the second polarisation on the minimum bow force would be expected to depend on the timing of the bow force oscillations relative to the moment within the cycle when the perturbation force at the bowing point reaches its maximum value: this is the critical moment for determining the minimum bow force.

Time-domain simulations of four cases are compared to investigate how this effect varies with the properties of the body modes and over different frequencies. The chosen base case relates to the single-polarisation vibration of a damped but perfectly flexible $D_3$ cello string, terminated at a body with a single resonance at 172 Hz with an effective mass of 300 g (consistent with the cases plotted in Fig. 11b). This relatively lightly-coupled case is chosen to limit variations in bowing-point admittance and to focus instead on the effects that bow force fluctuations have on the friction force. For simplicity, the torsional motion of the string is excluded. The results will be compared with other cases that bring in the second polarisation of string motion. The body mode is inclined with

respect to the bowing direction by $\theta_M = +20°$ in one case, and by $\theta_M = -20°$ in the other, both with the same adjustment to maintain the effective mass in the bowing direction at 300 g. To monitor the effects caused by variations in bowing-point admittance, a fourth case is considered that is the same as the case with $\theta_M = +20°$ except the fluctuations of the bow force are not considered in the calculation of friction.

Given that for all dual-polarisation cases the coupling happens via a single mode whose frequency is also close to the played note, the second polarisation of the string mainly responds to the fundamental frequency of the string. Simulation results, not reproduced here, show that the bow force reaches its maximum at a time close to the stick-to-slip transition for playing frequencies below the body mode, whereas it reaches its maximum value at around the middle of the sticking phase for frequencies above it. The same pattern is expected for the perturbation force at the bowing point: the body acts like a spring (in-phase vibration) at frequencies below its mode frequency and like a mass (out-of-phase vibration) at frequencies above it. Based on the argument given above, a body mode with $\theta_M > 0$ should reduce the minimum bow force at all frequencies (because it produces a larger value for the effective bow force when the perturbation force reaches its maximum). The corresponding computations for the $\theta_M = -20°$ case resulted in an exact reversal of the relative timing, so the prediction would be an increase in minimum bow force at all frequencies.

Figure 13 provides simulation results that show how well those predictions work. The relative number of double-slip/decaying occurrences for each played note of the three dual-polarisation cases are compared to that for the base case: a larger number of such samples indicates a relatively larger minimum bow force. As expected, the $\theta_M = +20°$ case has a significantly smaller number of double-slip/decaying samples than the base case; the opposite holds for the $\theta_M = -20°$ case. The minimum bow force for the case with $\theta_M = +20°$ but a constant bow force remains very close to that of the single polarisation case except at the relative frequency +1.99 Hz: this confirms the suggestion that the influence of bow force fluctuations is generally stronger than the effect of admittance changes. The reader is warned not to over-interpret these results: the range of simulations was obviously the same for any given played note for the four different cases, but it was different for different played notes. So, for example, green bars for different notes should not be directly compared to one another.

It should be noted that the effect of $\theta_M$ will be negated by reversing the bowing direction (i.e. from up-bow to down-bow). For a real instrument at lower frequencies, the center of rotation for the bridge is usually close to the bridge foot on the treble side [27]. As a result, for ergonomically possible bow inclinations the body modes generally have slightly positive angles for the lowest string (e.g. $C_2$ for the cello) and negative angles for all other strings.

# 5 Discussion and Conclusions

The minimum bow force needed to sustain the Helmholtz regime on a bowed string has been extensively studied as a useful measure of "playability" variations between instruments or between notes on a given instrument. Schelleng's original formula gave a useful first approximation, but one that was hard to apply quantitatively to any specific instrument. Woodhouse [4] extended the argument to make use of the measured bridge admittance on a given instrument, resulting in quantitative note-by-note predictions. In this paper, that approach has been further refined to take account of observed changes in the waveform of force applied by the string at the bridge when playing a note close to a strong body resonance.

Starting from an assumption of a perfect stick-slip velocity waveform at the bow, rather than a perfect sawtooth force excitation at the bridge as before, these waveform variations can be understood and predicted. The predictions, together with the corresponding revised relation for the minimum bow force, have been very successfully validated by extensive time-domain simulations. A striking feature of the new predictions is that the minimum bow force can depend on the bowing position $\beta$ in a far more complicated way than in the earlier models: in extreme cases, it is even predicted that there might be a "playability gap": a range of $\beta$ where Helmholtz motion cannot be sustained, although it becomes possible by bowing either nearer to the bridge or further from the bridge.

A combination of analysis and simulation has also been used to investigate the influence on the minimum bow force of several aspects of bowed-string physics that were ignored in the simpler calculations. It had been previously suggested by various authors that torsional motion of the string might have an effect on minimum bow force, by modifying the characteristic admittance of the string felt by the bow. However, it has been shown that this modification is not appropriate: detailed simulations agree more closely with estimates of minimum bow force that ignore torsion than they do with supposedly "improved" estimates incorporating the modified admittance. This can be attributed to the fact that the first torsional mode of a finite-length string has a much higher frequency than that of the first transverse mode, so the detailed admittance at the bowing point at low frequencies is very little perturbed by torsional effects.

The effect of sympathetic strings and their interactions with the body modes has been examined. Modes of sympathetic strings can sometimes have a significant influence, usually confined to frequencies

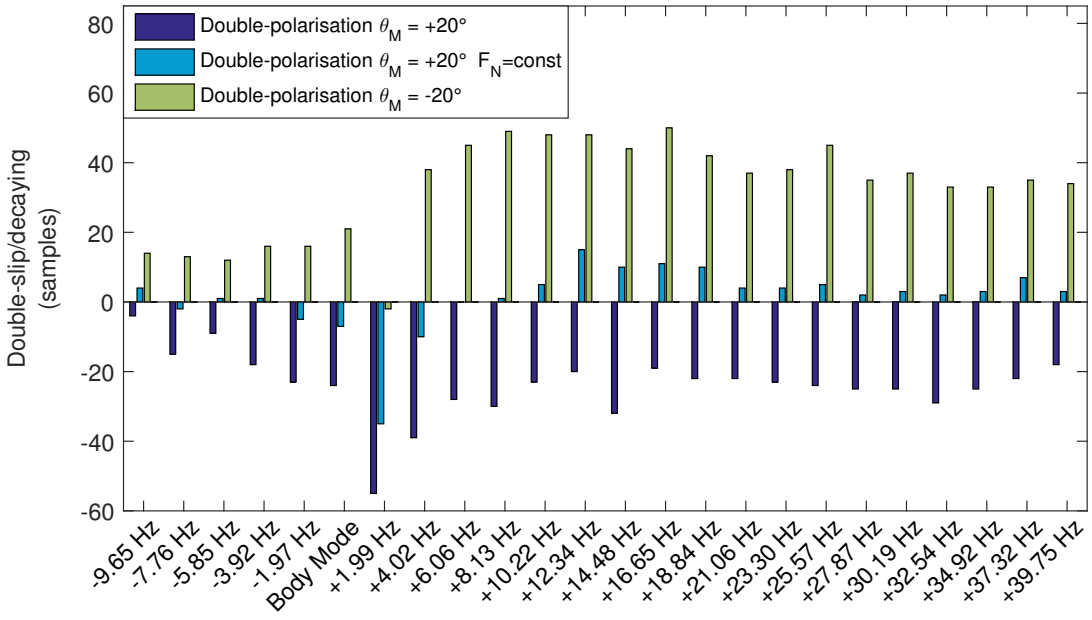


Figure 13: The relative number of double-slip/decaying samples out of a total of 600 simulated samples for each string frequency. The numbers are for the three cases of double-polarisation with respect to the single-polarisation base case. The double-polarisation cases include $\theta_M = +20°$, $\theta_M = -20°$, and $\theta_M = +20°$ but without considering the fluctuations of bow force. The horizontal axis shows the frequency of the simulated note relative to the body mode frequency. See the text for the description details of the simulations.

where there is some close harmonic relation between modes of the played and sympathetic strings. It is easy to modify the bridge admittance to take account of the effect of sympathetic strings (including the after-lengths of strings on the non-played side of the bridge). That modified admittance can be incorporated directly in the calculation of the minimum bow force.

Finally, the influence of the second polarisation of transverse string has been examined. Such influence can come by two routes: by modifying the admittance of the string at the bowed point, or by causing fluctuations in the force in the normal direction (on top of the player's imposed bow force). Both mechanisms can have effects that might, under some circumstances, be noticed by a player, but under normal circumstances the effects seem to be quite minor.

# 6 Acknowledgment

The authors are grateful to the anonymous reviewers for their valuable comments. The first author would like to acknowledge the government of Canada for a Vanier Canada Graduate Scholarship.

# References

[1] H. Helmholtz, *On the sensations of tone*. Dover Publications (English translation of the German edition was published in 1954), 1877.

[2] C. V. Raman, "Experiments with mechanically-played violins," *Proceedings of the Indian Association for the Cultivation of Science*, vol. 6, pp. 19–36, 1920.

[3] J. C. Schelleng, "The bowed string and the player," *The Journal of the Acoustical Society of America*, vol. 53, no. 1, pp. 26–41, 1973.

[4] J. Woodhouse, "On the playability of violins. Part II: Minimum bow force and transients," *Acustica*, vol. 78, pp. 137–153, 1993.

[5] R. T. Schumacher and J. Woodhouse, "The transient behaviour of models of bowed-string motion," *Chaos: An Interdisciplinary Journal of Nonlinear Science*, vol. 5, no. 3, pp. 509–523, 1995.

[6] E. Schoonderwaldt, K. Guettler, and A. Askenfelt, "An empirical investigation of bow-force limits in the schelleng diagram," *Acta Acustica united with Acustica*, vol. 94, no. 4, pp. 604–622, 2008.

[7] R. T. Schumacher, "Measurements of some parameters of bowing," *The Journal of the Acoustical Society of America*, vol. 96, no. 4, pp. 1985–1998, 1994.

[8] J. H. Smith and J. Woodhouse, "The tribology of rosin," *Journal of the Mechanics and Physics of Solids*, vol. 48, no. 8, pp. 1633–1681, 2000.

[9] J. Woodhouse, "Bowed string simulation using a thermal friction model," *Acta Acustica united with Acustica*, vol. 89, no. 2, pp. 355–368, 2003.

[10] H. Mansour, J. Woodhouse, and G. Scavone, "Time-domain simulation of the bowed cello string: Dual-polarization effect," in *Proceedings of Meetings on Acoustics*, vol. 19, p. 035014, Acoustical Society of America, 2013.

[11] J. C. Schelleng, "The violin as a circuit," *The Journal of the Acoustical Society of America*, vol. 35, pp. 326–338, March 1963.

[12] W. Reinicke, *Die Übertragungseigenschaften des Streichinstrumentensteges*. PhD thesis, Technical University of Berlin, 1973.

[13] P. M. Galluzzo, *On the playability of stringed instruments*. Thesis, Engineering Department, University of Cambridge, Cambridge, UK, 2003.

[14] A. Zhang and J. Woodhouse, "Reliability of the input admittance of bowed-string instruments measured by the hammer method," *The Journal of the Acoustical Society of America*, vol. 136, no. 6, pp. 3371–3381, 2014.

[15] L. Cremer, "Das Schicksal der 'Sekundärwellen' bei der Selbsterregung von Streichinstrumenten (translated: The fate of 'secondary waves' arising from self-excitation of stringed instruments)," *Acta Acustica united with Acustica*, vol. 42, no. 3, pp. 133–148, 1979.

[16] H. Mansour, *The bowed string and its playability: Theory, simulation and analysis*. Thesis, Department of Music Research, McGill University, Montreal, Canada, 2016.

[17] H. Mansour, J. Woodhouse, and G. P. Scavone, "Enhanced wave-based modelling of musical strings. Part 1: Plucked strings," *Acta Acustica united with Acustica*, vol. 102, no. 6, pp. 1082–1093, 2016.

[18] H. Mansour, J. Woodhouse, and G. P. Scavone, "Enhanced wave-based modelling of musical strings. Part 2: Bowed strings," *Acta Acustica united with Acustica*, vol. 102, no. 6, pp. 1094–1107, 2016.

[19] B. Lawergren, "Harmonics of s motion on bowed strings," *The Journal of the Acoustical Society of America*, vol. 73, no. 6, pp. 2174–2179, 1983.

[20] C. Valette, "The mechanics of vibrating strings," in *Mechanics of musical instruments* (A. Hirschberg, ed.), pp. 115–183, Springer-Verlag, Vienna, 1995.

[21] R. Mores, "Maximum bow force revisited," *The Journal of the Acoustical Society of America*, vol. 140, no. 2, pp. 1162–1171, 2016.

[22] J. P. Den Hartog, *Mechanical vibrations*. Dover Publications Reprint of 4th ed. Published by McGraw-Hill 1956, 1985.

[23] R. M. Foster, "A reactance theorem," *Bell System Technical Journal*, vol. 3, no. 2, pp. 259–267, 1924.

[24] C. E. Gough, "The theory of string resonances on musical instruments," *Acustica*, vol. 49, no. 2, pp. 124–141, 1981.

[25] G. Weinreich, "Coupled piano strings," *The Journal of the Acoustical Society of America*, vol. 62, no. 6, pp. 1474–1484, 1977.

[26] C. E. Gough, "The resonant response of a violin G-string and the excitation of the wolf-note," *Acta Acustica united with Acustica*, vol. 44, no. 2, pp. 113–123, 1980.

[27] A. Zhang, J. Woodhouse, and G. Stoppani, "Motion of the cello bridge," *The Journal of the Acoustical Society of America*, vol. 140, no. 4, pp. 2636–2645, 2016.